*International Journal for Uncertainty Quantification*, 5 (5): 433–451 (2015)

# AN UNCERTAINTY VISUALIZATION TECHNIQUE USING POSSIBILITY THEORY: POSSIBILISTIC MARCHING CUBES

***Yanyan He,[1,*] Mahsa Mirzargar,[1] Sophia Hudson,[1] Robert M. Kirby,[1,2] & Ross T. Whitaker[1,2]***

[1] *Scientific Computing and Imaging Institute, University of Utah, Salt Lake City, UTAH 84112, USA*
[2] *School of Computing, University of Utah, Salt Lake City, UTAH 84112, USA*

[*] Address all correspondence to Yanyan He E-mail: yhe@sci.utah.edu

*Original Manuscript Submitted: 04/06/2015; Final Draft Received: 09/30/2015*

*This paper opens the discussion about using fuzzy measure theory for isocontour/isosurface extraction in the field of uncertainty visualization. Specifically, we propose an uncertain marching cubes algorithm in the framework of possibility theory, called possibilistic marching cubes. The proposed algorithm uses the dual measures—possibility and necessity—to represent the uncertainty in the spatial location of isocontour/isosurface, which is propagated from the uncertainty in ensemble data. In addition, a novel parametric way of constructing marginal possibility distribution is proposed so that the epistemic uncertainty due to the limited size of the ensemble is considered. The effectiveness of the proposed possibilistic marching cubes algorithm is demonstrated using 2D and 3D examples.*

**KEY WORDS:** *representation of uncertainty, possibility theory, marching cubes, isosurface extraction, possibilistic marching cubes, uncertainty visualization*

## 1. INTRODUCTION

With the increase in the complexity and dimensionality of data used in a wide variety of applications ranging from simulation sciences to medical application, domain experts and scientists are using visualization to enhance and accelerate the task of data analysis. The visualization community has been designing techniques and algorithms for proper visual representation of various types of data and features extracted from them. Among different data types often used in practice, scalar fields are an often-used data type found in applications. Isocontours in 2D and isosurfaces in 3D are the main features oftentimes extracted from scalar fields and visualized using the celebrated *marching cubes* algorithm [1]. The algorithm, for example in 3D, extracts a piecewise linear surface (i.e., in terms of a triangular mesh) that best approximates the underlying isosurface, which is then visualized through a rendering pipeline.

Because uncertainty is an inevitable component of modeling, simulation and data acquisition, and various sources of uncertainty—including inaccuracy in the physical measurements, model inaccuracy, uncertain parameters, and many more—can undermine the scientific pipeline, many scientific communities have acknowledged the need for studying and quantifying the uncertainty present in their work flow. The visualization community is not immune to these trends. The uncertainty associated with the data fed into the visualization pipeline can affect the quality and accuracy of the visual representation of the data. Therefore, taking into account the uncertainty present in the data is necessary to design effective visualization techniques.

According to the sources, uncertainty can be broadly categorized into two types: *aleatory* and *epistemic*. Aleatory uncertainty, also known as statistical (chance) uncertainty, is due to the inherent randomness of the processes, while

2152–5080/15/$35.00  

epistemic uncertainty, known as systematic uncertainty, is considered to be a consequence of a lack of knowledge [2]. Probability theory has been well developed and considered as the only choice for modeling uncertainty in applications until the recognition of epistemic uncertainty. Recent advances in uncertainty quantification have suggested that studying uncertainty strictly in a probabilistic framework may not be appropriate for all situations [3]. It has also been noticed that probability theory is designed to model random effects, and its ability to capture or represent *lack of knowledge* could therefore be limited [4]. As a result, alternative mathematical frameworks need to be explored for uncertainty quantification. In the past few decades, modern mathematical frameworks such as fuzzy set theory [5], possibility theory [6], and evidence theory [7] have been proposed as ways of quantifying incomplete knowledge [8] and successfully applied to various fields, such as visualization [9–11], image processing [12], risk assessment [13], data fusion [14], etc.

With an increasing interest in uncertainty quantification techniques, visualization of uncertainty (or uncertainty visualization) has begun to attract attention [15–19]. Different taxonomies [15, 20] have been defined for proper representation of uncertainty via different visual channel encodings including color, glyphs, and blurriness [21–23]. Various visualization techniques have been proposed to help users study the variability in their data. For instance, Ensemblevis [24] is designed to convey statistical properties of ensemble data. Noodles [25] is an example of a domain-specific technique to visualize ensembles of weather forecast data. Direct visualization of ensembles has also been studied and has been shown to be an effective scheme for visualizing uncertainty in hurricane track prediction [26].

Most proposed uncertain visualization techniques use probability theory as their theoretical building block, to model uncertainty present in the data prior to visualization [19, 21, 27–29]. Isosurface extraction is considered to be one of the primary building blocks of many visualization schemes, and therefore, visualization of uncertain isosurfaces has received significant attention. For instance, in order to quantify and visualize the uncertainty in isosurfaces extracted from scalar fields, parametric density estimation techniques have been used to approximate level crossing probabilities (LCP) [27, 28, 30]. The concept of LCP has been generalized to take into account the local correlation structure of the ensemble data in [19] and [30]. We will introduce the former one proposed by Pöthkow et al. [19] later in detail and call it the probabilistic marching cubes algorithm (PMC). We will discuss PMC in detail in the next section. More probability theory based visualization techniques can be found in the literature [31–34].

As mentioned earlier, probability theory may not always be suitable for quantifying uncertainty in applications. Therefore, it is necessary to explore the application of alternative mathematical frameworks to uncertainty visualization. This paper extends the widely used visualization technique—marching cubes—in the framework of a fuzzy measure theory: possibility theory. The main contributions of the current manuscript can be summarized as:

- Opening the discussion of using a fuzzy measure theory—possibility theory—for isosurface extraction.
- Proposing a novel way of constructing possibility distribution to represent the uncertainty in ensemble data.
- Quantifying the positional uncertainty of an isosurface using possibility theory in the marching cubes pipeline.

The remainder of the paper proceeds as follows. In the next section, we will provide the background of conventional marching cubes and probability marching cubes. Section 3 is devoted to an introduction to possibility theory, where we introduce the basic concepts, propose a novel way of constructing possibility distribution and discuss the decision making based on the measures in possibility theory. We then propose the mathematical and computational aspects of our new algorithm: *possibilistic marching cubes* (PossMC) in Section 4. In Section 5, we provide a canonical 2D example to show the theoretical properties of the proposed PossMC algorithm, as well as two 2D applications (one fluid mechanics example and one weather prediction example) and a 3D synthetic example to demonstrate the effectiveness of PossMC algorithm. We summarize and conclude our work in Section 6.

## 2. BACKGROUND OF MARCHING CUBES

In this section, we provide a detailed introduction to the conventional marching cubes algorithm, which is designed for extraction of isosurfaces from deterministic scalar fields and, hence, we call it deterministic marching cubes. Then we introduce its probabilistic generalization proposed for quantification and visualization of the uncertainty present in isosurfaces extracted from uncertain scalar fields.

As mentioned in Section 1, isosurface extraction is a versatile technique for visualizing scalar fields. A scalar field can be considered as a discrete representation of an unknown multivariate function $f(\vec{x})$ evaluated on a grid. For the simplicity of discussion, we consider 3D scalar fields on a Cartesian lattice where each grid cell is a cube and the scalar values of the scalar field reside on the eight corners. However, the marching cubes algorithm can be easily generalized to any structured or unstructured grid in any dimension. An isosurface in 3D is defined as the level set of the multivariate function that gives rise to the scalar field, and as the set of points in the domain for which the underlying multivariate function attains a specific isovalue, $\theta$: $C = \{\vec{x} \in \mathbb{R}^3 | f(\vec{x}) = \theta\}$. Since a scalar field is a discrete representation of the underlying multivariate function at grid points, the marching cubes algorithm uses a trilinear approximation (i.e., tensor product of univariate linear interpolation) to estimate the underlying function at any arbitrary point, and then extracts the isosurface associated with the chosen isovalue.

The deterministic marching cubes algorithm proceeds as follows: at each grid cell, a decision needs to be made as to whether there exists level crossing in that cell or not. Based on the trilinear assumption that coincides with linear interpolation along each of the edges of the grid cell (i.e., a cube), the marching cubes algorithm determines the presence of level crossings with respect to a chosen isovalue based on the values of the scalar field at the corners of the cell. For instance, if the values of the scalar field are all above (or below) the chosen isovalue, the level crossing cannot happen inside the cell (considering the trilinear approximation of the underlying multivariate function). Therefore, level crossing at a grid cell can happen only if there exists at least one sign change with respect to the chosen isovalue at the corners of the cell, i.e., there exist two corners of the cell such that the value at one corner is above while the value of the other one is below the chosen isovalue. In this case, the marching cubes algorithm determines a polygonal representation of the isosurface passing through the cell. More specifically, the level crossings over edges are hashed to a particular approximating tessellation. The polygonal representation of the isosurface (i.e., equivalent to piecewise linear representation of the isosurface) can lead to non-unique tessellation (ambiguity) [35]. The inherent ambiguity problem with the marching cubes algorithm has been well-studied and addressed [36].

In the presence of uncertainty, however, the conventional marching cubes algorithm may not provide accurate information about the spatial location of the isosurface as the data values at each grid location are no longer deterministic. In order to alleviate this problem and account for the uncertainty associated with ensemble data of scalar fields, a probabilistic version of the marching cubes algorithm was proposed in [19]. The probabilistic marching cubes (PMC) algorithm uses an ensemble of instances of scalar fields as an empirical version of a stochastic multivariate function (or field of data). The uncertainty in this case is modeled by assigning a random variable to each of the grid points. Instead of extracting the exact position of the isosurface, PMC algorithm determines the probability of the presence of the isosurface at each grid cell. The PMC algorithm considers a parametric local correlation model for each grid cell. The joint distribution at each cell is defined as a multivariate Gaussian function whose parameters (i.e., the sample mean and covariance matrix) are determined based on the ensemble values at the corners of each cell. The joint probability distribution at each grid cell is then used to approximate the probability of the presence of a level crossing in each cell using a Monte Carlo sampling from the joint probability distribution associated with each cell (i.e., multivariate Gaussian function). When applied to ensemble data, the PMC algorithm provides quantitative information regarding the uncertainty associated with the spatial location of isosurface in terms of the level crossing probability values for each cell. Visualization of level crossing probability overlaid with the mean isosurface (or isocontour in 2D) has been proposed as a visualization technique for isosurfaces extracted from uncertain scalar fields [19].

The ensemble data of scalar fields from which one extracts isosurfaces contain a finite number of samples at each grid point. According to Iaccarino [37], "the use of a finite number of samples from a population leads to epistemic uncertainty." As mentioned earlier, probability theory may not be appropriate to quantify different types of uncertainty, and consequently PMC may not always be suitable. Therefore, it is necessary to explore the uncertain marching cubes algorithms using other mathematical frameworks. To open the discussion about applying fuzzy measure theories (or more broadly, dealing with different types of uncertainty) in isosurface extraction, we adopt a simple and relatively well-developed fuzzy measure theory—possibility theory—to develop an uncertain marching cubes algorithm, i.e., to quantify the positional uncertainty of isosurfaces of scalar fields. In the next section, we present a brief introduction to possibility theory.

## 3. INTRODUCTION TO POSSIBILITY THEORY

### 3.1 Basics of Possibility Theory

Possibility theory is mathematically the simplest uncertainty theory for dealing with incomplete information [4]. It is a natural means for quantifying epistemic uncertainty coming from lack of knowledge. In this section, we will introduce the basics of possibility theory necessary for the development of our method.

#### 3.1.1 Possibility Distribution

Let $Y$ denote a variable, analogous to a random variable in probability theory, that takes on values from a set $U$ containing the true value. In our work, $Y$ takes real numbers as values, i.e., $U \subseteq \mathbb{R}$. If we know the true value of $Y$, then our knowledge is complete, and there is no uncertainty. However, we may have only partial knowledge, and hence the true value of $Y$ is unknown. In what follows, we will adopt the terminology used in the possibility literature [4]. Many of the terms we use colloquially (such as possible, unsurprising, etc.) will take on precise mathematical meaning.

In this case, a possibility distribution can be constructed to represent the incomplete information about the value of $Y$ ranging on $U$. The possibility distribution $\pi_Y$ assigns a number in the unit interval $[0, 1]$ to each element $u \in U$. The possibility value describes the degree to which it is *possible* that the element $u$ is the true value of $Y$. When $\pi_Y(u) = 0$, $Y = u$ is considered as an *impossible* situation; when $\pi_Y(u) = 1$, $Y = u$ is considered as *unsurprising*, a much weaker statement than when $p(Y = u) = 1$, where $p$ denotes a probability function [4]. Since the set $U$ contains the true value, there exists $u \in U$ such that $\pi_Y(u) = 1$. One example of a possibility distribution $\pi_Z$ for an unknown variable $Z$ is shown as the dashed line in Fig. 1(a), from which we can tell that we would be unsurprised if $Z = 0.5$, given that $\pi_Z(0.5) = 1$. It is impossible for $Z < -1$ or $Z > 1$ since the degree of possibility is zero.

As noted by Zadeh [38], the possibility distribution defined in possibility theory is numerically equal to the concept of membership functions (which quantifies the grade of membership of an element within a fuzzy set) in fuzzy set theory [5].

#### 3.1.2 Joint Possibility Distribution

Let $\pi_Y(y)$ and $\pi_Z(z)$ be marginal possibility distributions for two uncertain variables $Y$ and $Z$. Then the joint possibility distribution $\pi_{Y,Z}(y, z)$ is defined as [39]

$$\pi_{Y,Z}(y, z) = T(\pi_Y(y), \pi_Z(z)), \tag{1}$$

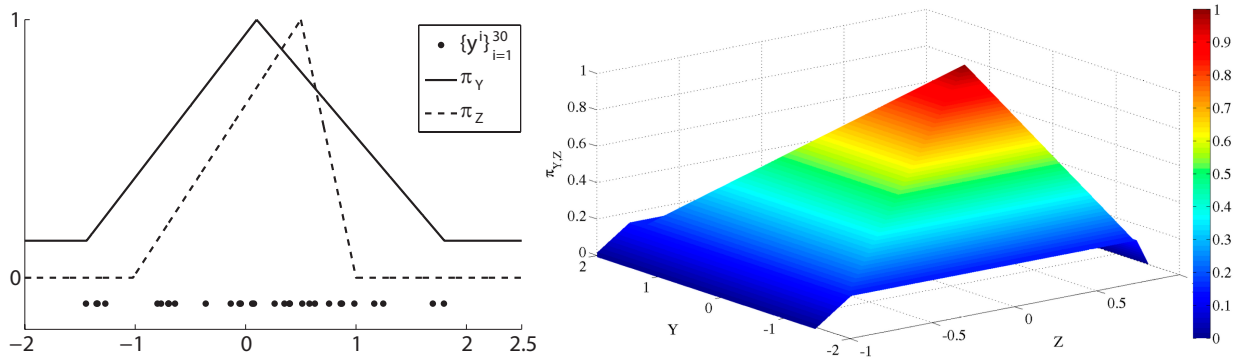


(a) (b)

**FIG. 1:** Examples of marginal and joint possibility distributions: (a) the possibility distributions for variables $Y$ and $Z$, respectively, (b) the joint possibility distribution for variables $Y$ and $Z$. Sample values $y^i$ from which the possibility distribution for $Y$ can be inferred are shown as dots along the horizontal axis.

where $T$ is a $t$ norm, defined as a function $T : [0, 1] \times [0, 1] \rightarrow [0, 1]$, which satisfies

1. Commutativity $T(a, b) = T(b, a)$;
2. Monotonicity $T(a, b) \leq T(c, d)$ if $a \leq c$ and $b \leq d$; and
3. Associativity $T(a, T(b, c))) = T(T(a, b), c)$.

There are various $t$ norm definitions in the literature [39], and they mainly differ from each other in the way they associate. The choice of a specific $t$ norm depends on the application scenario and the choice affects the shape of the joint possibility distribution [39]. In the current work, we assume that the uncertain variables are independent. Under such an assumption, the following "min" $t$ norm should be used [38, 40]:

$$T(a, b) = \min\{a, b\}.$$

In addition, the "min" $t$ norm is a special case of the Frank $t$ norm family [39], which has been shown particularly suitable for the construction of the joint possibility distribution by comparing the resulting joint possibility distribution using Frank $t$ norm family and a reference joint possibility distribution transferred from a joint probability distribution [39].

An example of a joint possibility distribution of variables $Y$ and $Z$ is shown in Fig. 1. With the marginal possibility distributions in Fig. 1(a) as $\pi_Y(y)$ and $\pi_Z(z)$, using the "min" $t$-norm, the joint possibility distribution $\pi_{Y,Z}(y, z)$ is obtained and shown in Fig. 1(b).

The joint possibility distribution of three independent variables $Y_1, Y_2, Y_3$ is obtained as follows:

$$\begin{aligned}\pi_{Y_1,Y_2,Y_3}(y_1, y_2, y_3) &= T(\pi_{Y_1}(y_1), \pi_{Y_2,Y_3}(y_2, y_3)),\\ &= T(\pi_{Y_1}(y_1), T(\pi_{Y_2}(y_2), \pi_{Y_3}(y_3))),\\ &= T(T(\pi_{Y_1}(y_1), \pi_{Y_2}(y_2)), \pi_{Y_3}(y_3)).\end{aligned}$$

Extended to $N$ independent variables $Y_1, Y_2, ..., Y_N$, the joint possibility distribution is given by

$$\pi_{Y_1,Y_2,...,Y_N}(y_1, y_2, ..., y_N) = T(T(...T(\pi_{Y_1}(y_1), \pi_{Y_2}(y_2)), ...), \pi_{Y_N}(y_N)).$$

Although there have been a few attempts in the literature to discover the correlation between uncertain variables represented by possibility distributions [41], it is still an open problem to construct joint distribution for correlated variables in applications. Therefore, we assume the independent relation among variables in the current work and leave the dependent scenario for future research.

### 3.1.3 Possibility and Necessity

In possibility theory, the terms *possibility* and *necessity* are used to quantify the uncertainty due to incomplete information. Let $A \subseteq U$ be any subset of $U$ and consider the proposition "the true value of the quantity $Y$ belongs to the subset $A$." For simplicity, we use $A$ to represent the proposition hereafter. The possibility measure, $Poss(A)$, provides the degree of possibility that the value of $Y$ belongs to the subset $A$. It is defined as a number in $[0, 1]$ given by

$$Poss(A) = \max_{u \in A} \pi_Y(u). \tag{2}$$

The possibility measure has the following properties:

1. $Poss(\emptyset) = 0$;
2. $Poss(U) = 1$ if $\exists u \in U$ such that $\pi_Y(u) = 1$;
3. $Poss(A \cup B) = \max\{Poss(A), Poss(B)\}$, for $A, B \subseteq U$.

The dual of a possibility measure is called a necessity measure, defined as

$$Nec(A) = 1 - Poss(A^c), \tag{3}$$

where $A^c$ is the complement of the subset $A$. Equation (3) implies that proposition $A$ is necessarily true if and only if the complement of $A$ is impossible. A necessity measure satisfies $Nec(A \cap B) = \min\{Nec(A), Nec(B)\}$.

Necessity measure $Nec(A)$ quantifies the strength of data supporting proposition $A$ while the possibility measure $Poss(A)$ measures the maximum possible support from the data to proposition $A$. Fig. 2 illustrates graphically the relaxation of additivity for these two measures, i.e., $Nec(A) + Nec(A^c) \leq 1$ and $Poss(A) + Poss(A^c) \geq 1$. The gray area describes the epistemic uncertainty in proposition $A$, and $[Nec(A), Poss(A)]$ can be viewed as the range of possible strength of support for proposition $A$. Compared to the superadditivity of necessity measure, probability theory has strict additivity: $P(A) + P(A^c) = 1$. The additivity in probability theory indicates that the epistemic uncertainty represented by the gray area of Fig. 2 disappears. Thus probability theory is natural for quantifying aleatory uncertainty, and possibility theory is suitable for quantifying epistemic uncertainty.

### 3.2 Constructing Possibility Distribution from Ensemble Data

One special scenario of uncertainty quantification is to represent the uncertainty in the ensemble data $\{y^i\}_{i=1}^n$ (i.e., construct the distribution from data) associated with a random variable $Y$, whose probability density function is unknown. If there are infinitely many samples available for the random variable, one can construct a probability density function accurately. However, in practice, we may have the situation where a limited number of samples are available. We consider such a situation in the current work and construct a possibility distribution to represent the uncertainty in the incomplete information. There are various ways to construct a possibility distribution in the literature [42, 43]. We adopt the simple parametric one with triangular shape [42] [e.g., the dashed line $\pi_Z$ in Fig. 1(a)], which captures certain characteristics of the ensemble data, such as mean and lower and upper bounds. However, the strict triangular shape considers the values outside the range of ensemble data impossible, which may not be realistic especially when the ensemble size $n$ is small.

We propose the following way (a modified version of triangular shape) to construct a possibility distribution for the variable $Y$:

$$\pi_Y(y) = \begin{cases} 1 - \dfrac{(y - y_{mean})(1 - p^+)}{y_{\max} - y_{mean}} & \text{if } y_{mean} \leq y \leq y_{\max} \\ p^+ + \dfrac{(y - y_{\min})(1 - p^+)}{y_{mean} - y_{\min}} & \text{if } y_{\min} \leq y < y_{mean} \\ p^+ & \text{otherwise} \end{cases}, \tag{4}$$

where $y_{mean}$ is the sample mean of the ensemble data, $y_{\min}$ represents $\min\{y^i\}_{i=1}^n$, $y_{\max}$ denotes $\max\{y^i\}_{i=1}^n$; we assign $p^+$ to $\pi_Y(y)$ for any $y \in (-\infty, y_{min}) \cup (y_{max}, \infty)$ since it is quite possible that the true value of $Y$ falls outside the ensemble range $[y_{min}, y_{max}]$. The value (of possibility distribution) $p^+$ indicates how much possible that $Y$ takes a value outside the ensemble range.

The $p^+$ is defined using the simultaneous confidence interval proposed by Quesenberry et al. [44] and Goodman [45] as follows:

$$p^+ = \frac{a + 2n + \sqrt{D}}{2(N + a)}, \tag{5}$$

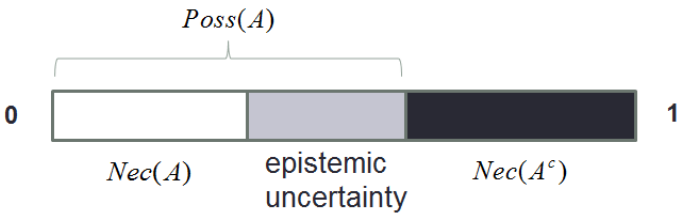


**FIG. 2:** Necessity and possibility of proposition $A$.

where $a$ is the quartile of order $1-\alpha$ of the chi-square distribution with one degree of freedom, $n=0$ is the number of ensemble data points falling outside of the ensemble, $N$ is the size of ensemble, and $D=a(a+4n(N-n)/N)$.

The defined $p^+$ satisfies $p(0 \leq p(Y \notin [y_{\min}, y_{\max}]) \leq p^+) \geq 1-\alpha$, i.e., the probability that the chance of "the value of $Y$ falls outside of the ensemble range" is less than $p^+$ is no less than $1-\alpha$. Therefore, $p^+$ can be considered as the upper bound of probability of $Y$ falling outside the ensemble range. It is reasonable to assign $p^+$ to the possibility distribution because if so, $Poss(Y \notin [y_{\min}, y_{\max}])) = p^+$ holds and the degree of possibility can be considered as upper bound of probability. In the current work, we take one of the usual probability levels $\alpha = 0.025$.

We also have $p^+ \in (0,1]$. When the ensemble size is zero (i.e., $N=0$), no information is available, $p^+=1$ and consequently $\pi_Y(y)=1$ for all $y \in \mathbf{R}$, this scenario is called total ignorance; while the ensemble size is getting large (e.g., $N \to \infty$), $p^+ \to 0$ and $\pi_Y(y)$ has the triangular shape.

For example, Fig. 1(a) shows the constructed possibility distribution $\pi_Y$ (the solid line) from the ensemble data $\{y^i\}_{i=1}^N$ with size $N=30$. The proposed method of constructing possibility distributions is based on the triangular shape and is easy to implement. In addition, it considers the situation where the true value is outside of the ensemble range, which could be very common when the ensemble size is small.

### 3.3 Decision-Making Using Possibility and Necessity Measures

The possibility distributions are constructed at the credal level where possibility and necessity measures are used to quantify the uncertainty. However, to make decisions, Smets observed that one might need to transfer the fuzzy measure into a probability function, and he defined the associated pignistic probability distribution ($BetP$) for the measures in evidence theory [46, 47]. Because possibility theory can be considered as one special case of evidence theory, we adopt the concept and definition of pignistic probability distribution for possibility/necessity measures as follows.

Let $Poss : 2^{\mathbf{X}} \to [0,1]$ and $Nec : 2^{\mathbf{X}} \to [0,1]$ be the dual fuzzy measures—possibility and necessity—in possibility theory, where the universal set $\mathbf{X}$ contains the finite number of possible outcomes (i.e., $|\mathbf{X}| < \infty$). Then the pignistic probability distribution of the proposition $A \subseteq \mathbf{X}$ is defined as

$$BetP(A) = Nec(A) + \frac{Poss(A) - Nec(A)}{2}. \tag{6}$$

Note that the pignistic probability distribution $BetP$ is calculated from possibility and necessity values. The concept of $BetP$ is not necessary for uncertainty quantification in the framework of possibility theory, and it only facilitates decision-making. In general, in the situation where it may not be straightforward to conclude the preference over propositions using upper and lower bounds (possibility and necessity values), the pignistic probability can be considered as an estimation of the true probability to help make decisions.

## 4. POSSIBILISTIC MARCHING CUBES (POSSMC)

In this section, we will establish the mathematical foundation required to model the positional uncertainty of an isosurface using the possibility theory framework and introduce the notion of *level crossing possibility*. We then devise an efficient algorithm to compute level crossing possibility values. The comparisons among the mathematical theories for uncertainty modeling and among the corresponding marching cubes algorithms are beyond the scope of the current manuscript.

### 4.1 Level crossing Possibility

Without any loss of generality, we construct a joint possibility distribution and introduce the concept of level crossing possibility for an edge in 1D, and then demonstrate how one can extend it to higher dimensions.

Consider two adjacent points $X_1$ and $X_2$ as corners of an edge associated with sets of ensemble data $\{y_1^i\}_{i=1}^{n_1}$ and $\{y_2^i\}_{i=1}^{n_2}$, respectively. One can construct the marginal possibility distributions $\pi_{Y_j}(y_j)$ for $Y_j$ $(j = 1, 2)$ individually using the proposed method in Section 4. Once the possibility distributions associated with the two points are obtained, we can use the "min" $t$ norm to construct the joint possibility distribution for the edge as

$$\pi_{Y_1,Y_2} = \min(\pi_{Y_1}(y_1), \pi_{Y_2}(y_2)). \tag{7}$$

To compute the level crossing possibility for an isovalue θ, one needs to calculate the possibility that both signs occur in the set of differences $\{Y_k - \theta\}_{k=1,2}$. The level crossing possibility is defined as

$$Poss(\theta\text{-}crossing) = Poss(\{Y_1 \geq \theta, Y_2 \leq \theta\} \cup \{Y_1 \leq \theta, Y_2 \geq \theta\}), \tag{8}$$

where $Poss(\theta\text{-}crossing)$ denotes the level crossing possibility. The level crossing regions $A_1 = \{Y_1 \leq \theta, Y_2 \geq \theta\}$ and $A_2 = \{Y_1 \geq \theta, Y_2 \leq \theta\}$ are demonstrated in Fig. 3(a). Using the properties of a possibility measure defined in the previous section, Eq. (8) can be rewritten as

$$Poss(\theta\text{-}crossing) = \max\{Poss(A_1), Poss(A_2)\} = \max\left\{\max_{A_1} \pi_{Y_1,Y_2}(y_1, y_2), \max_{A_2} \pi_{Y_1,Y_2}(y_1, y_2)\right\}.$$

Note that this formulation of the level crossing possibility values entails an optimization problem that could be expensive to compute in higher dimensions. In fact, using this naive implementation of the algorithm with sampling method for optimization, the computational cost is exponential: $(2^d - 2)n^d$, where $d$ denotes the number of corners of a cell (e.g., $d = 2$ for an edge) and $n$ is sample size in the optimization process. However, in the following theorem, we prove that the level crossing possibility values can be evaluated using an efficient optimization, whose computational cost is $(2^d - 2)dn$. The naive implementation of edge-crossing possibility values over the regions specified in Fig. 3 results in a 2D optimization problem, while using the method following from the theorem, one can compute the edge-crossing possibility values by solving two 1D optimization problems.

**Theorem 1.**
Let $Y_1$,$Y_2$ be two independent variables associated with possibility distributions $\pi_{Y_1}(y_1)$ over $U_1$ and $\pi_{Y_2}(y_2)$ over $U_2$, respectively, and let $T$ be the "min" $t$ norm. If $A$ is the Cartesian product of $S_1$ and $S_2$ (i.e., $A = S_1 \times S_2$), where $S_1 \subseteq U_1$ and $S_2 \subseteq U_2$. Then

$$Poss(A) = T\left(\max_{S_1} \pi_{Y_1}(y_1), \max_{S_2} \pi_{Y_2}(y_2)\right). \tag{9}$$

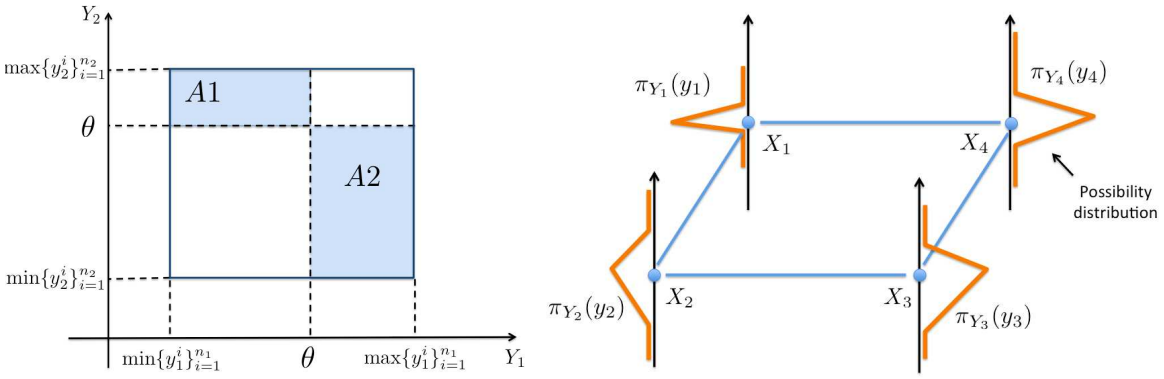


(a) (b)

**FIG. 3:** Illustrations of (a) different level crossing regions for an edge in 1D, (b) the construction of possibility distributions for the four variables at the corner of a rectangle in 2D.

*Proof.* The theorem can be proved through application of the monotonicity property of $t$ norms [4].

$$\begin{aligned} Poss(A) &= \max_A \pi_{Y_1,Y_2}(y_1, y_2), \\ &= \max_A T(\pi_{Y_1}(y_1), \pi_{Y_2}(y_2)), \qquad (10) \\ &\leq T\left(\max_{S_1} \pi_{Y_1}(y_1), \max_{S_2} \pi_{Y_2}(y_2)\right), \qquad (11) \\ &= T(\pi_{Y_1}(y_1^\star), \pi_{Y_2}(y_2^\star)), \qquad (12) \end{aligned}$$

where $y_1^\star$ is the value that maximizes $\pi_{Y_1}(y_1)$ over the set $S_1$, and $y_2^\star$ is the value that maximizes $\pi_{Y_2}(y_2)$ over the set $S_2$. Since $A = S_1 \times S_2$, we have $(y_1^\star, y_2^\star) \in A$, and consequently the following inequality holds:

$$T(\pi_{Y_1}(y_1^\star), \pi_{Y_2}(y_2^\star)) \leq \max_A T(\pi_{Y_1}(y_1), \pi_{Y_2}(y_2)). \qquad (13)$$

Therefore the equality in Eq. (11) holds. □

### 4.1.1 Two-Dimensional Case

For computing the level crossing possibilities in 2D, we need to consider $N = 4$ variables $Y_1, Y_2, Y_3, Y_4$ at four grid points $X_1, X_2, X_3, X_4$ (the corners of a square). The variables are associated with four sets of ensemble data, based on which the possibility distributions $\pi_{Y_1}, \pi_{Y_2}, \pi_{Y_3}, \pi_{Y_4}$ are constructed, respectively [see Fig. 3(b)].

Let the binary number "1" indicate $Y_i \geq \theta$ and "0" indicate $Y_i \leq \theta$. Then, the $2^N - 2 = 14$ level crossing regions can be represented using binary numbers (see Table 1). The level crossing possibility is then defined as

$$Poss(\theta\text{-}crossing) = Poss(\cup_{i=1}^{14} A_i) = \max\{Poss(A_1), ..., Poss(A_{14})\}.$$

With $\vec{y} = \{y_1, y_2, y_3, y_4\}$, Theorem 1 can be intuitively extended to the setting of $N = 4$ independent variables:

**TABLE 1:** The 14 different level crossing regions $\{A_i\}_{i=1}^{14}$ in 2D

| Regions | Binary number |
|---|---|
| $A_1$ | 0001 |
| $A_2$ | 0010 |
| $A_3$ | 0011 |
| $A_4$ | 0100 |
| $A_5$ | 0101 |
| $A_6$ | 0110 |
| $A_7$ | 0111 |
| $A_8$ | 1000 |
| $A_9$ | 1001 |
| $A_{10}$ | 1010 |
| $A_{11}$ | 1011 |
| $A_{12}$ | 1100 |
| $A_{13}$ | 1101 |
| $A_{14}$ | 1110 |

$$
\begin{aligned}
Poss(A_i) &= \max_{\{\vec{y}\in A_i\}} \pi_{Y_1,Y_2,Y_3,Y_4}(y_1,y_2,y_3,y_4) \\
&= \max_{\{\vec{y}\in A_i\}} T(T(T(\pi_{Y_1},\pi_{Y_2}),\pi_{Y_3}),\pi_{Y_4}) \\
&= T\left(\max_{\{y_1,y_2,y_3|\vec{y}\in A_i\}} T(T(\pi_{Y_1},\pi_{Y_2}),\pi_{Y_3}), \max_{\{y_4|\vec{y}\in A_i\}} \pi_{Y_4}(y_4)\right) \\
&= T\left(T\left(\max_{\{y_1,y_2|\vec{y}\in A_i\}} T(\pi_{Y_1},\pi_{Y_2}), \max_{\{y_3|\vec{y}\in A_i\}} \pi_{Y_3}\right), \max_{\{y_4|\vec{y}\in A_i\}} \pi_{Y_4}\right) \\
&= T\left(T\left(T\left(\max_{\{y_1|\vec{y}\in A_i\}} \pi_{Y_1}, \max_{\{y_2|\vec{y}\in A_i\}} \pi_{Y_2}\right), \max_{\{y_3|\vec{y}\in A_i\}} \pi_{Y_3}\right), \max_{\{y_4|\vec{y}\in A_i\}} \pi_{Y_4}\right).
\end{aligned}
$$

#### 4.1.2 Three-Dimensional Case

In order to compute the level crossing possibility value in 3D, we need to consider $N = 8$ independent variables at the eight corners of a cube, $\{Y_i\}_{i=1}^{N=8}$. Their marginal possibility distributions are then constructed individually from their corresponding ensemble data using the proposed method, following which, the possibility of a level crossing at an isovalue θ is computed as the maximum possibility value on $2^8 - 2$ different level crossing regions. The possibility on each level crossing region can be calculated using the extension of Theorem 1. This formulation can equivalently be extended to higher dimensions.

### 4.2 Implementation

Here we discuss several important aspects of the computation of the level crossing possibility values and provide pseudocode of the Algorithm 1.

**Algorithm 1:**

At each grid cell with $N$ corners
**Data**: Ensemble data set $\{y_i^k\}_{k=1}^{n_i}$ at all corners indexed with $i = 1, ..., N$
**Result**: $Poss(\theta\text{-}crossing)$
**while** $i \leq N$ **do**
  construct the possibility distribution $\pi_i$ for $i$ th corner using Eq. (4);
  return the degrees of possibility of the chosen sampling points;
  classify the sampling points into set "1" or "0";
**end**
let $Poss(\theta\text{-}crossing) = 0$;
**while** $j \leq 2^N - 2$ **do**
  from the binary representation of $A_j$, find the corresponding set of samples at $i$ th corner for $i = 1, ..., N$;
  obtain the maximum degree of possibility $\tilde{\mu}_i$ over the corresponding set;
  calculate the possibility $Poss = T(...T(\tilde{\mu}_1, \tilde{\mu}_2), ..., \tilde{\mu}_N)$;
  update $Poss(\theta\text{-}crossing) = max\{poss(\theta\text{-}crossing), poss\}$;
**end**
$Nec(\theta\text{-}crossing) = 1 - Poss((\theta\text{-}crossing)^c)$.

As mentioned previously, a possibility distribution function $\pi_i$ at $i$ th grid point is constructed from the ensemble data set $\{y_i^k\}_{k=1}^{n_i}$. To solve the optimization problem using the sampling method, we evaluate the degrees of possibility at the chosen sampling points based on $\pi_i$s. We then use the binary number (such as "0001" in 2D and "00000001" in 3D) to classify the combinations of sampling points at all the corners into different level crossing regions $\{A_i\}$. Specifically, the sampling points for each corner (or node) are classified into the set "1" if the value is greater than or equal to θ or the set "0" if the value is less than θ. For example, in 2D, $A_1$ = "0001" contains all the combinations of the sampling points from the sets "0" at the lower-left, lower-right, up-left corners and the set "1" at the up-right corner,

i.e., $A_1 = \{Y_1, Y_2, Y_3, Y_4 | Y_1 < \theta, Y_2 < \theta, Y_3 < \theta, Y_4 \geq \theta\}$. With the possibility distribution and classification at all the corners of each grid cell, we compute the possibility of each level crossing region $A_i$ using Theorem 1 or its extension to 2D/3D.

The possibilistic marching cubes algorithm needs to consider all the level crossing cases because of the relaxation of the additivity constraint; however, it benefits from efficient evaluation of the level crossing possibility values over the regions of crossing, without the need for Monte Carlo sampling from the joint distribution required for PMC.

## 5. RESULTS AND APPLICATIONS

In this section, we demonstrate with four experimental examples (with both 2D and 3D datasets since marching cubes algorithm can be generalized to any structured or unstructured grid in any dimensions) the utility of our uncertainty visualization technique based on cell-crossing possibility and necessity values in representing the uncertain isocontours/isosurfaces. We will start with a synthetic example, and then demonstrate the results for two real-life applications from computational fluid dynamics and weather forecast. We then implement the proposed PossMC algorithm on a 3D synthetic dataset to show that the algorithm is applicable to a high-dimensional dataset. We also provide the PMC isocontour result for the computational fluid dynamics application for reference. In all the examples, the colormap has been scaled so that the highest level crossing possibility/necessity/probability value is assigned to red and the minimum level crossing possibility/necessity/probability value is assigned to white. This scaling of the colormap helps to provide a better color contrast.

Note: As mentioned in Section 2, due to the aleatory uncertainty, one cannot extract the exact position of the isocontour/isosurface (i.e., obtain the deterministic isocontour/isosurface); the best one can do is to calculate and visualize the probability of the presence of the isocontour/isosurface at each grid cell. In the situation where both epistemic and aleatory uncertainties exist, one may not be able to estimate (and consequently visualize) the probability of level crossing accurately, but we can calculate the possibility and necessity of level crossing which bound the true probability and visualize them. In other words, it can be understood as that the aleatory uncertainty is shown as multiple locations of isocontours with different degrees of possibility or necessity (visualized in different colors); and the epistemic uncertainty is shown as the difference between the degrees of necessity and possibility at each cell.

### 5.1 Synthetic Test Dataset

Our 2D (size $512 \times 512$) synthetic dataset consists of an ensemble of size $30$. We used an implicit formulation of a diamond as $|x| + |y| \leq r$ and generated the ensemble by varying the value of $r$ using a normally distributed random value with a mean value of $2.0$ and standard deviation of $0.4$. In order to construct a nontrivial and interesting example, each ensemble member has been contaminated with correlated random noise.

The level crossing possibility/necessity values have been computed for an isovalue of $\theta = 0.5$, and the possibilities have been visualized in Fig. 4(a) and the necessities are zero for all the cells. The possibility and necessity of level crossing over the whole field represent the uncertainty in the spatial location of isocontour, which is propagated from the uncertainty in the ensemble data. Figure 4(a) indicates the region (in red) that has relatively higher maximum chance (i.e., the higher possibility values) to have level crossing. However, as mentioned before, it may not be straightforward (or one may not feel comfortable) to make decisions regarding the spatial location of an isocontour based on the comparison of the maximum chance of level crossing. Therefore, we also calculate their corresponding pignistic probability distribution $BetP$ (shown as Fig. 4(b)) from possibility and necessity values to help make decisions. The pignistic probability distribution shows the region (in red) with the highest pignistic probability to have level crossing, which is coincident with the region with the highest possibility values due to zero necessities.

We are also interested in comparing the result from PossMC to the true probability of level crossing. To estimate the true probability of level crossing, we construct the 2D synthetic dataset of an ensemble with size $1000$, and then calculate the ratio of the number of level crossing to the total size $1000$ [visualized in Fig. 4(c)]. The dataset of the ensemble of size $30$, which we used to demonstrate the proposed PossMC and calculate the results shown in Figs. 4(a) and 4(b), is a subset of the constructed ensemble with size $1000$. From Figs. 4(b) and 4(c), one can easily observe that both pignisitc probability from PossMC and the true probability are relatively large for the same region.

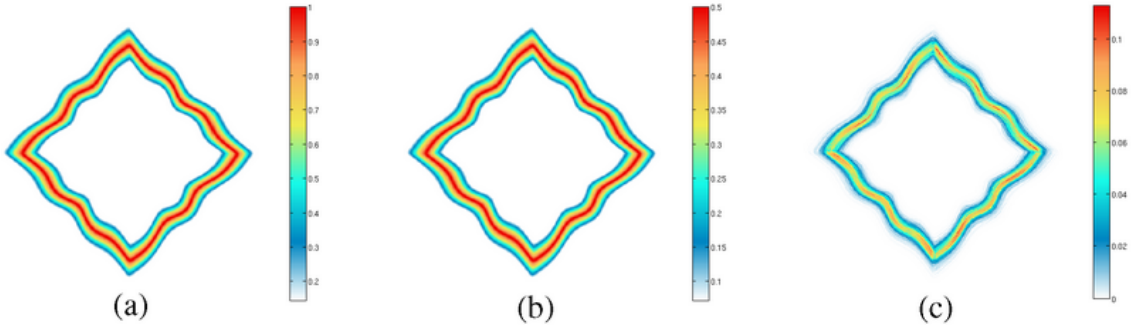


**FIG. 4:** Synthetic ensemble data: (a) possibilistic marching cubes visualization, (b) pignistic probabilistic marching cubes, and (c) true probability of level crossing.

In addition, we compare the possibility values to the true probability values. Figure 5(d) shows the level crossing possibility and true probability values for the cells at the 250th row. From this, one can tell that (1) the level crossing possibility is greater than the true level crossing probability, which is consistent with the theoretical point of view: the possibility can be viewed as upper probability bound; (2) the possibilities are nonzero (equal to $p^+$) where the true probabilities are zero, which reflects the consideration of the proposed PossMC algorithm on the epistemic uncertainty due to the limited size of the ensemble; (3) the possibilities are much larger than the true probabilities when they are nonzero, one of the possible reasons would be that we constrain the possibility distribution based on the triangle shape with a maximum value of one.

## 5.2 Real-World Two-Dimensional Examples

### 5.2.1 Fluid Mechanics Example

Our second set of results is motivated by the study of vortices in a computation fluid dynamics (CFD) application where scientists are interested in the size, number, and position of the vortices present in a flow field generated by the presence of an obstacle. When the fluid passes an obstacle, the eddies or vortices are formed in a periodic fashion and move in the direction of the flow field as shown in Fig. 6. One of the simplest approaches for studying vortex structures in a flow field is to study its pressure field (as a proxy for vorticity). The center of a vortex typically corresponds to minimum pressure values. Therefore, isocontours of the pressure field can be used to approximate the position of

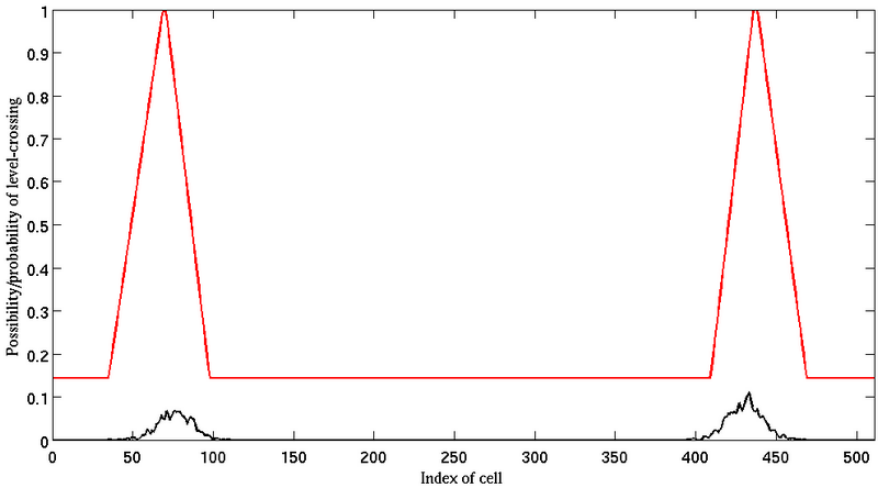


**FIG. 5:** Comparison of possibilistic values to true probabilistic values.

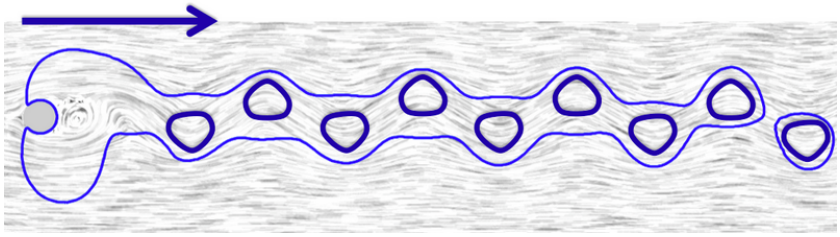

**FIG. 6:** Eddy (vortex) lines in one fluid simulation: the flow direction is from left to right where the approximate position of the eddies has been specified by dark circles, the blue curve represents the isocontour associated with the pressure value $-0.005$, and the pressure isocontour provides an *envelope* representing the approximate position of the vortices.

the vortices in a flow field. The behavior of vortices in this simple setting is well studied in terms of parameters such as Reynolds number, initial conditions, and boundary conditions, but in an experimental setting, the presence of uncertainty in the parameters, initial conditions, and boundary conditions is unavoidable. In order to mimic the uncertainty present in the parameters of a real fluid simulation, we generated an ensemble of simulation runs for the fluid flow scenario shown in Fig. 6.

For this example, we used the 2D incompressible Navier-Stokes solver as part of the Nektar++ software package [48] to generate simulation results for fluid passing a stationary obstacle (in this case a cylinder). We generated our ensemble of size $40$ by random perturbation of the inlet velocity and the Reynolds number. Changing the Reynolds number and the inlet velocity will translate into a scaling of the pressure values. We performed a preprocessing step in order to normalize the pressure field of each ensemble member based on the average of the pressure value for a unique and fixed point inside the field behind the cylinder. After normalization of the pressure field for all ensemble members, we used isovalue = $-0.005$ for isocontour extraction.

Similar to our canonical example, we calculate the level crossing possibility and necessity values of the pressure field of the flow and visualize them in Figs. 7(b) and 7(d). The possibility value indicates the maximum chance of level crossing at each cell and the region near the outflow boundary (in red) has a relatively higher maximum chance of level crossing. The contour with nonzero necessity values [Fig. 7(d)] is coincident with the ensemble mean isocontour. Since the contour is almost invisible in the flow background, Fig. 7(d) uses a plain color background to have more contrast between the contour and background. The level crossing possibility and necessity values over the whole field represent the uncertainty in the spatial location of the pressure isocontour. For the purpose of decision-making, we also provide the pignistic probability of level crossing calculated from possibilities and necessities. Figure 7(c) shows that the region near the outflow boundary with light green color (besides the region around the obstacle) has a relatively higher pignistic probability of level crossing.

For this example, in addition to level crossing possibility/necessity values, we also provided the direct ensemble visualization of the isocontours of the pressure field in Fig. 7(a). The direct ensemble visualization demonstrates the higher levels of variability among the ensemble members in the region near the outflow boundary, and the pignistic probability result calculated from possibility and necessity values is consistent with the result of the direct ensemble visualization.

### 5.2.2 Weather Forecast Example

Ensembles of simulation runs are heavily used in climate and weather forecasting in order to account for both model and parameter uncertainty. The National Oceanic and Atmospheric Administration (NOAA) provides various publicly available ensemble data for weather forecast applications [50]. For this example, we use the SREF-CONUS (40 km) temperature ensemble consisting of $21$ ensemble members. The ensemble members are generated using three forecast model runs with seven perturbations of the initial conditions to account for the uncertainty present in the initial conditions of the simulation. We have chosen to use one of the predefined temperature isovalues adopted by NOAA. The temperature value for this experiment is given as $-15°$C at $500$ mb.

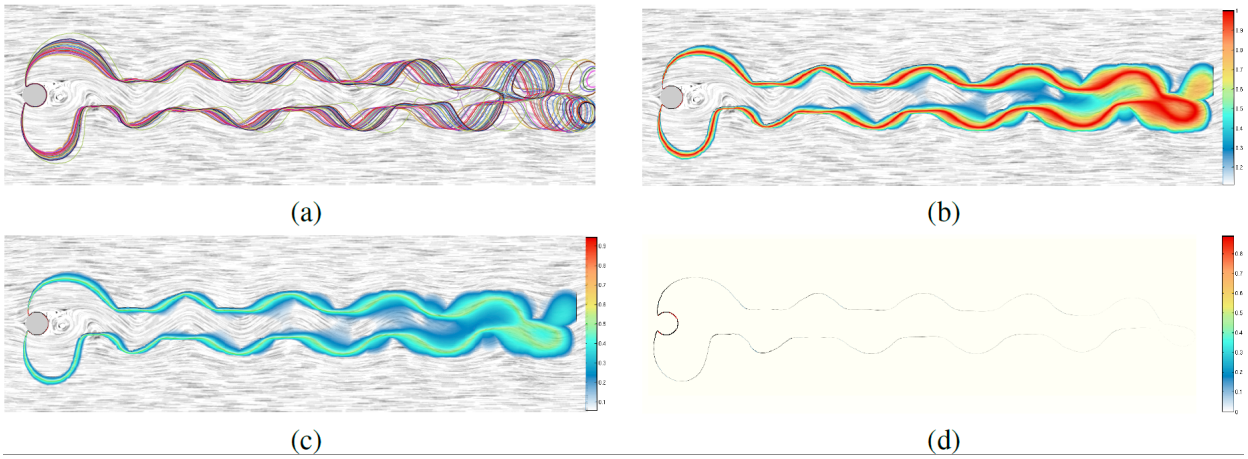


**FIG. 7:** Uncertain isocontours of the pressure field: (a) Ensemble of isocontours of the pressure field extracted from fluid simulation. (b) Possibilities (from PossMC) visualization. (c) Pignistic probabilities (from PossMC) visualization. (d) Necessities (from PossMC) visualization (the contour is faded looking due to the chosen colorbar: small necessity values are represented by white and light blue colors). The visualization has been overlaid on top of a LIC [49] visualization of one of the ensemble members.

Figure 8 provides the visualization of the level crossing possibility and necessity values as well as the level crossing pignistic probability values. Possibility and necessity values can be considered as the upper and lower bounds of the true probability of level crossing at each cell, and pignistic probability values can be used as the approximation of the true probability for decision-making. From Fig. 8(b), one can easily extract the domain with a higher chance of level crossing (the domain in orange-yellow) out from the whole domain in consideration.

In the following, we demonstrate on a three-dimensional example that the PossMC algorithm is applicable for high-dimensional cases.

### 5.3 Three-Dimensional Example

The proposed possibilistic marching cubes algorithm is naturally extendable to higher-dimensional cases. In this example, we provide the results of the PossMC algorithm for the synthetic 3D example given in [19] through volume rendering of the level crossing possibility/necessity values. The synthetic data contain an ensemble of $45$ volumetric data using the analytical formula:

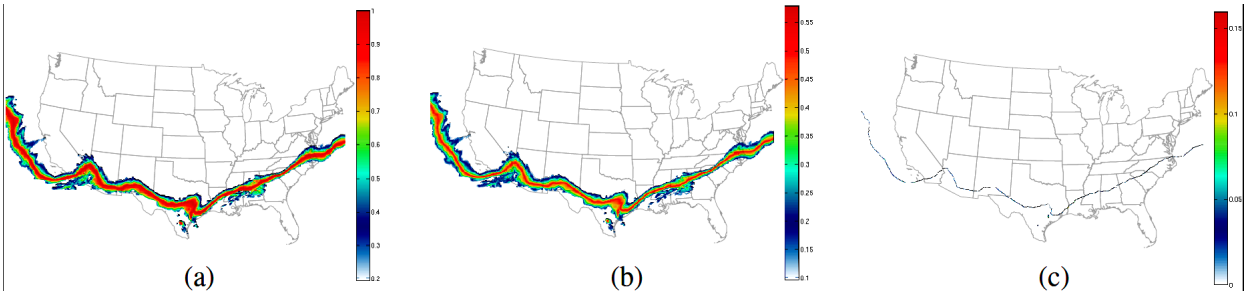


**FIG. 8:** Visualization of uncertain isocontours of temperature fields from CONUS at $500$ mb at temperature $-15°$C: (a) Possibilities (from PossMC) visualization. (b) Pignistic probabilities (from PossMC) visualization. (c) Necessities (from PossMC) visualization (the contour is faded looking due to the chosen colorbar: small necessity values are represented by white and light blue colors).

$$\mu(x, y, z) = (\cos(7x) + \cos(7y) + \cos(7z))\exp(ar), \quad \text{where } r = \sqrt{x^2 + y^2 + z^2}, \quad a = -4.5. \tag{14}$$

Each ensemble member is a volume of size $300 \times 300 \times 250$ where $a$ has been perturbed by adding normally distributed noise values. Similar to the 2D examples, the volume rendering of the level crossing possibility values is consistently higher than that of the necessity values [visualized in Figs. 9(a) and 9(c)], which reflects the theoretical result that possibility viewed as the upper bound of the true probability is always larger than the necessity considered as the lower bound. Both the possibility and necessity values over the whole domain represent the uncertainty in the spatial location of the isosurface. To help make decisions about the uncertain isosurface, we approximate the true probability of level crossing with the pignistic probability calculated from possibility and necessity values. The pignisitc probability of level crossing at each cube is visualized in Fig. 9(b), the spatial locations with relatively greater pignistic probability values (in red-yellow color) have a higher chance to constitute the isosurface with isovalue $\theta = 0.0013$.

### 5.4 The Results of Probabilistic Marching Cubes on Fluid Mechanics Example

As mentioned previously, the construction of possibility distribution from correlated ensemble is still an open problem. We assume the uncorrelated relation in the current work. However, we would like to explore how the correlation might impact the uncertain isosurface extraction. In this section, we apply both the original PMC algorithm, which considers the correlation between corners in each cell using multivariate normal distribution, and the uncorrelated version of the PMC algorithm to the first real-world example—fluid mechanics. We implement the uncorrelated version of the PMC algorithm by assigning zeros to the off-diagonal correlation coefficients for each cell, which can be considered as a special case of the previous study on LCP under the stochastic dependence assumption [27]. Then we compare the results from the two versions of PMC to study the impact of the correlation.

The result from uncorrelated version of PMC algorithm is visualized as Fig. 10(a) and the one from the original PMC algorithm is shown in Fig. 10(b). Due to the correlation, the probability that the isocontour passes each cell is relatively smaller compared to the one from the uncorrelated version, which matches one's intuition: the correlated grid points tend to have similar values, for instance, if one of the grid points has a value greater than the isovalue; its correlated grid points also tend to have values greater than the isovalue. Consequently there will be less chance of level crossing. Especially in the region close to outflow boundaries, the probability of level crossing from original PMC becomes very small, which makes it less informative to help make decisions regarding the spatial location of pressure isocontour. In addition, observe that in the region above the centerline at the outflow boundary [the region marked with a square in Fig. 10(a)], there exist nonzero level crossing probability values (from uncorrelated version) that are not present (or very low) in the original PMC visualization (correlated version). The probability of the presence of level crossings from the uncorrelated version in this region is consistent with the results of the direct ensemble

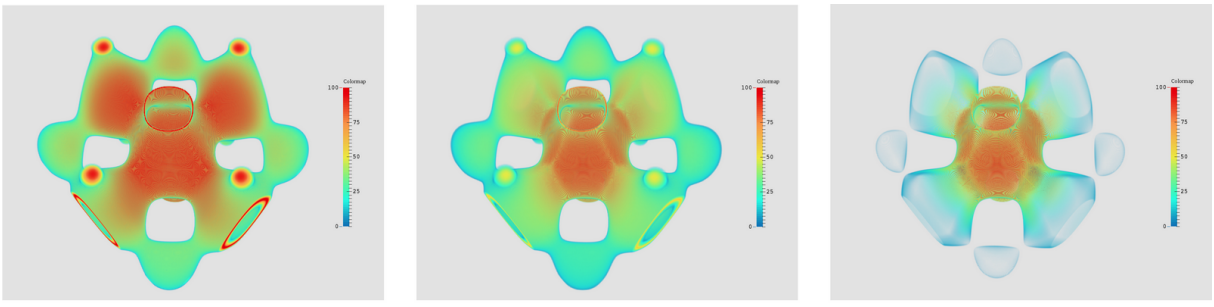

(a) (b) (c)

**FIG. 9:** Uncertain isosurface visualization of a synthetic 3D dataset. (a) Volume rendering of the possibility values of level crossing for $\theta = 0.0013$ calculated using the PossMC algorithm. (b) Volume rendering of the pignistic probability values of level crossing for $\theta = 0.0013$ calculated using the PossMC algorithm. (c) Volume rendering of the necessity values of level crossing for $\theta = 0.0013$ calculated using the PossMC algorithm. In all cases the transparency increases as the data values decrease.

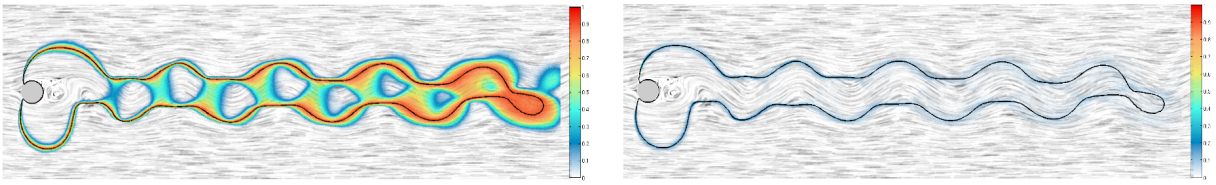

(a) (b)

**FIG. 10:** Isocontours of the pressure field extracted from fluid simulation: (a) Probabilities visualization from uncorrelated version of PMC. (b) Probabilities visualization from PMC. The visualization has been overlaid on top of a LIC [49] visualization of one of the ensemble members. The mean isocontour is rendered as a black curve in both visualizations.

visualization. This effect is not a result of outliers, as the analysis in [33] confirms the high chance of level crossing in this region.

However, Fig. 10(a) shows that the uncorrelated PMC algorithm assigns relatively high nonzero probability values to the region between the subsequent vortices (the region marked with an ellipse), which is not consistent with the direct ensemble visualization [see Fig. 7(a)]. The original PMC algorithm (correlated version) assigns zero degrees of probability to the region between the subsequent vortices, which matches the ensemble visualization. Therefore, it would be interesting to develop a correlated version of the PossMC algorithm in future research and it is hoped that the designed correlated version of PossMC can capture more characteristics of the ensemble data.

For all the results, the level crossing possibility and probability values were computed using MATLAB, where the computational time for each 2D example is about 1 min. The computational cost of PossMC algorithm is dominated by the number of cells and hence a parallel implementation of the algorithm can significantly increase the efficiency.

## 6. SUMMARY AND CONCLUSIONS

Proper characterization of the uncertainty associated with an ensemble is a challenging problem. Even though probabilistic methods are oftentimes applied to the quantification and visualization of uncertainty, the probabilistic modeling of uncertainty may not be always the best choice. In this paper, we open the discussion about using fuzzy measure theories in isocontour extraction. Specifically, we introduce the mathematical foundations required to model the uncertainty in an ensemble using a fuzzy measure theory—possibility theory; and propose a new characterization of an uncertain isosurface through the introduction of the concept of level-crossing possibility/necessity and possibilistic marching cubes visualization.

Through 2D and 3D examples, we have illustrated the theoretical properties of the proposed possibilistic marching cubes algorithm, and demonstrated that the PossMC algorithm is capable of quantifying the uncertainty associated with ensemble data, and consequently the calculated possibility and necessity values are able to represent the uncertainty in the spatial location of isocontour/isosurface. We also provide the result from the probabilistic marching cubes algorithm for one example as a reference, which indicates that the correlation between nodes can have an effect on the spatial location of the isocontour/isosurface.

Since this work is one of the very first efforts at incorporating fuzzy measure theories to isosurface extraction, the proposed PossMC algorithm has made an assumption of the independent relation. To the best of our knowledge, constructing the joint possibility distribution for dependent uncertain variables is an open question and hence provides an interesting direction for future research. In addition, we construct the marginal possibility distribution from ensemble data using a particular parametric approach (based on a triangular shape). In the future, we would like to incorporate the nonparametric approaches (i.e., without assuming any basic shapes) of constructing possibility distributions into the PossMC algorithm, which may provide a route for improving the quality and accuracy of the computed level-crossing possibility.

## ACKNOWLEDGMENTS

The second and fifth authors acknowledge the support of National Science Foundation (NSF) grant IIS-1212806. The third author acknowledges REU support under the same NSF grant. The first and fourth authors acknowledge support by the Army Research Laboratory under Cooperative Agreement number W911NF-12-2-0023. The views and conclusions contained in this document are those of the authors and should not be interpreted as representing the official policies, either expressed or implied, of the Army Research Laboratory or the US Government. The US Government is authorized to reproduce and distribute reprints for Government purposes notwithstanding any copyright notation herein.

## REFERENCES

1. Lorensen, W. E. and Cline, H. E., Marching cubes: A high resolution 3d surface construction algorithm, *Comput. Graph.*, 21(4):163–169, 1987.
2. Hoffman, F. and Hammonds, J., Propagation of uncertainty in risk assessments: the need to distinguish between uncertainty due to lack of knowledge and uncertainty due to variability, *Risk Anal.*, 14(3):707–712, 1994.
3. Roy, C. J. and Oberkampf, W. L., A comprehensive framework for verification, validation, and uncertainty quantification in scientific computing, *Comput. Methods Appl. Mech. Eng.*, 200:2131–2144, 2011.
4. Dubois, D., Possibility theory and statistical reasoning, *Comput. Stat. Data Anal.*, 51(1):47–69, 2006.
5. Zadeh, L. A., Fuzzy sets, *Information Control*, (8):338–353, 1965.
6. Dubois, D. and Prade, H., *Possibility Theory*, Plenum Press, New York, 1988.
7. Shafer, G., *A Mathematical Theory of Evidence*, Princeton University Press, Princeton, NJ, 1976.
8. Swiler, L. P., Paez, T. L., and Mayes, R. L., Epistemic uncertainty quantification tutorial, In *Proceedings of the IMAC-XXVII*, Orlando, FL, February 2009.
9. Streit, A., Pham, B., and Brown, R., A spreadsheet approach to facilitate visualization of uncertainty in information., *IEEE Trans. Vis. Comput. Graph.*, 14(1):61–72, 2008.
10. Fout, N. and Ma, L., Fuzzy volume rendering, *IEEE Trans. Vis. Comput. Graph.*, 18(12):2335–2344, 2012.
11. Dahabiah, A., Puentes, J., and Solaiman, B., Possibilistic similarity estimation and visualization, In *Advances in Information Retrieval Theory*, pp. 273–280, Springer, New York, 2009.
12. He, Y., Hussaini, M. Y., Ma, J., Shafei, B., and Steidl, G., A new fuzzy c-means method with total variation regularization for segmentation of images with noisy and incomplete data, *Pattern Recognition*, 45(9):3463–3471, 2012.
13. Guyonnet, D., Bourgine, B., Dubois, D., Fargier, H., Come, B., and Chiles, J., Hybrid approach for addressing uncertainty in risk assessments, *J. Env. Eng.*, 129(1):68–78, 2003.
14. Chen, W., Cui, Y., He, Y., Yu, Y., Galvin, J., Hussaini, M. Y., and Xiao, Y., Application of Dempster-Shafer theory in dose response outcome analysis, *Phys. Med. Biol.*, 57(2):5575–5585, 2012.
15. Pang, A. T., Wittenbrink, C. M., and Lodh, S. K., Approaches to uncertainty visualization, *Visual Comput.*, 13:370–390, 1996.
16. Lodha, S., Wilson, C., and Sheehan, R., Listen: sounding uncertainty visualization, In *Proceedings of IEEE Visualization*, Los Alamitos, CA, pp. 189–195, November 1996.
17. Johnson, C. and Sanderson, A., A next step: Visualizing errors and uncertainty, *IEEE Comput. Graph. Appl.*, 23:6–10, 2003.
18. Athawale, T. and Entezari, A., Uncertainty quantification in linear interpolation for isosurface extraction, *IEEE Trans. Visual. Comput. Graph.*, 19(12):2723–2732, 2013.
19. Pöthkow, K., Weber, B., and Hege, H.-C., Probabilistic marching cubes, *Comput. Graph. Forum*, 30(3):931–940, 2011.
20. Potter, K., Rosen, P., and Johnson, C. R., From quantification to visualization: A taxonomy of uncertainty visualization approaches, In: Dienstfrey, A. and Boisvert, R. (Eds.), *Uncertainty Quantification in Scientific Computing*, Vol. 377 of IFIP Advances in Information and Communication Technology, pp. 226–249, Springer Berlin Heidelberg, 2012.
21. Grigoryan, G. and Rheingans, P., Probabilistic surfaces: Point based primitives to show surface uncertainty, In *Proceedings of IEEE Visualization*, Piscataway, NJ, pp. 147–153, October 2002.

22. Grigoryan, G. and Rheingans, P., Point-based probabilistic surfaces to show surface uncertainty, *IEEE Trans. Visualization and Computer Graphics*, 10:564–573, 2004.

23. Djurcilov, S., Kim, K., Lermusianax, P., and Pang, A., Visualizing scalar volumetric data with uncertainty, *Computers and Graphics*, 26:239–248, 2002.

24. Potter, K., Wilson, A., Pascucci, V., Williams, D., Doutriaux, C., Bremer, P.-T., and Johnson, C., Ensemble-vis: A framework for the statistical visualization of ensemble data, In *ICDMW '09. IEEE International Conference on*, Washington, DC, pp. 233–240, 2009.

25. Sanyal, J., Zhang, S., Dyer, J., Mercer, A., Amburn, P., and Moorhead, R., Noodles: A tool for visualization of numerical weather model ensemble uncertainty, *IEEE Transactions on Visualization and Computer Graphics*, 16(6):1421–1430, 2010.

26. Cox, J., House, D., and Lindell, M., Visualizing uncertainty in predicted hurricane tracks, *Int. J. Uncertainty Quantification*, 3(2):143–156, 2013.

27. Pöthkow, K. and Hege, H.-C., Positional uncertainty of isocontours: Condition analysis and probabilistic measures, *IEEE Transactions on Visualization and Computer Graphics*, 17(10):1393–1406, 2011.

28. Pöthkow, K., Petz, C., and Hege, H.-C., Approximate level-crossing probabilities for interactive visualization of uncertain isocontours, *Int. J. Uncertainty Quantification*, 3(2):101–117, 2013.

29. Petz, C., Pöthkow, K., and Hege, H.-C., Probabilistic local features in uncertain vector fields with spatial correlation, *Comput. Graph. Forum*, 31:1045–1054, 2012.

30. Pfaffelmoser, T., Reitinger, M., and Westermann, R., Visualizing the positional and geometrical variability of isosurfaces in uncertain scalar fields, *Comput. Graph. Forum*, 30(3):951–960, 2011.

31. Pfaffelmoser, T. and Westermann, R., Visualization of global correlation structures in uncertain 2D scalar fields, *Comput. Graph. Forum*, 31:1025–1034, 2012.

32. Pöthkow, K. and Hege, H.-C., Nonparametric models for uncertainty visualization, *Comput. Graph. Forum*, 32(3):131–140, 2013.

33. Whitaker, R. T., Mirzargar, M., and Kirby, R. M., Contour boxplots: A method for characterizing uncertainty in feature sets from simulation ensembles, *IEEE Trans. Visual. Comput. Graph.*, 19(12):2713–2722, 2013.

34. Mirzargar, M., Whitaker, R. T., and Kirby, R. M., Curve boxplot: Generalization of boxplot for ensembles of curves, *IEEE Trans. Visual. Comput. Graph.*, 20(12):2654–2663, 2014.

35. Natarajan, B., On generating topologically consistent isosurfaces from uniform samples, *Visual Comput.*, 11(1):52–62, 1994.

36. Nielson, G. M. and Hamann, B., The asymptotic decider: Resolving the ambiguity in marching cubes, In *Proceedings of the 2Nd Conference on Visualization '91*, IEEE Computer Society Press, Los Alamitos, CA, USA, pp. 83–91, 1991.

37. Iaccarino, G., Uncertainty quantification in computational science, http://web.stanford.edu/group/uq/events/pdfs/lecture_2.pdf. (Date of access: 04/01/2015)

38. Zadeh, L. A., Fuzzy sets as a basis for a theory of possibility, *Fuzzy Sets Syst.*, (1):3–28, 1978.

39. Ferrero, A., Prioli, M., and Salicone, S., The construction of joint possibility distributions of random contributions to uncertainty, *IEEE Trans. Instrument. Measur.*, 63(1):80–88, 2014.

40. Klir, G. and Yuan, B., *Fuzzy Sets and Fuzzy Logic: Theory and Applications*, Prentice-Hall Inc., Englewood Cliffs, NJ, 1995.

41. Carlsson, C., Fullér, R., and Majlender, P., On possibilistic correlation, *Fuzzy Sets Syst.*, 155(3):425–445, 2005.

42. Wang, E. and Shen, Z., A hybrid data quality indicator and statistical method for improving uncertainty analysis in LCA of complex system application to the whole-building embodied energy analysis, *J. Cleaner Production*, 43:166–173, 2013.

43. Blanchard, F., Vautrot, P., Akdag, H., and Herbin, M., Data representativeness based on fuzzy set theory, *J. Uncertain Syst.*, 3:216–228, 2010.

44. Quesenberry, C. P. and Hurst, D. C., Large sample simultaneous confidence intervals for multinomial proportions, *Technometrics*, 6(2):191–195, 1964.

45. Denœux, T., Constructing belief functions from sample data using multinomial confidence regions, *Int. J. Approx. Reasoning*, (42):228–252, 2006.

46. Smets, P., Data fusion in the transferable belief model, In *Proceedings of the Third International Conference on Information*

*Fusion*, Paris, France, July 2000.

47. Smets, P., Belief functions and the transferable belief model, http://www.sipta.org/documentation/belief/belief.ps. (Date of access: 04/01/2015)
48. Nektar++, http://www.nektar.info. (Date of access: 04/01/2015)
49. Cabral, B. and Leedom, L. C., Imaging vector fields using line integral convolution, In *Proceedings of the 20th Annual Conference on Computer Graphics and Interactive Techniques*, SIGGRAPH '93, ACM, New York, NY, USA, pp. 263–270, 1993.
50. National Oceanic and Atmospheric Administration, http://nomads.ncep.noaa.gov/. (Date of access: 08/31/2013)